SSRG International Journal of Electrical and Electronics Engineering
ISSN: 2348-8379/ https://doi.org/10.14445/23488379/IJEEE-V12I7P105

Volume 12 Issue 7, 73-85, July 2025

Original Article

A Non-Isolated Power Factor Correction Bridgeless High Gain Sepic Employing CPSO-PI Controller for Induction Motor Applications

A.A. Mohamed Faizal[1*], K. Murugesan[2], V. Thanka Jebarsan[3], S. Elanthamizh[4], R. Mageswaran[5], N. Janaki[6]

[1]*Department of Electrical and Electronics Engineering, V. V College of Engineering, Tamil Nadu, India.*
[2]*Department of Electrical and Electronics Engineering, Sri Siva Subramaniya Nadar College of Engineering, Tamil Nadu, India.*
[3]*Department of Civil Engineering, Noorul Islam Centre for Higher Education, Tamilnadu, India.*
[4]*Department of Electrical and Electronics Engineering, Sri Manakula Vinayagar Engineering College, Tamil Nadu, India.*
[5]*Department of Electrical and Electronics Engineering, S. A. Engineering College, Tamil Nadu, India.*
[6]*Department of Electrical and Electronics Engineering, Vels Institute of Science, Technology & Advanced Studies, Tamil Nadu, India.*

[1]*Corresponding Author : aamohamedfaizal106@gmail.com*

Received: 04 May 2025 Revised: 06 June 2025 Accepted: 05 July 2025 Published: 31 July 2025

Abstract - *Induction Motors (IMs) are widely employed in different industrial applications owing to their robustness and dependability. However, their operation often poses challenges in terms of Power Factor Correction (PFC) and voltage regulation, leading to inefficient energy utilization and harmonic distortions. Traditional PFC methods and voltage regulation techniques may not adequately address these issues. To overcome these issues, this paper develops a novel approach leveraging a non-isolated Bridgeless High Gain Single-Ended Primary Inductance Converter (SEPIC) with Chaotic Particle Swarm Optimization (CPSO) based Proportional Integral (PI) controller approach for IM applications. The proposed converter configuration aims to enhance power conversion efficiency and improve power factor with reduced Total Harmonic Distortion (THD). Furthermore, a control strategy termed a PI controller is employed to optimize the converter control performance, and the CPSO algorithm is introduced to optimally tune the PI parameters to achieve the desired settling time and rapid convergence speed performance, thereby enhancing the overall Efficiency and performance of IM. Furthermore, the developed topology is validated by utilizing MATLAB/Simulink, and the developed converter and control technique are compared with the other recent approaches to prove the greatness of the proposed system. The investigational outcomes prove that the proposed converter has reduced THD (1.98%), and the control technique performed better in terms of settling time and convergence speed. The developed work demonstrates its applicability and superiority for IM applications in terms of power quality enhancement and energy efficiency with a better PFC system.*

Keywords - *CPSO-PI controller, Induction motors, MATLAB/Simulink, Non-isolated bridgeless SEPIC converter, Power factor correction.*

1. Introduction

IMs are commonly used in different industrialized and commercial sectors owing to their robustness, reliability, and ease of control [1, 2]. However, their inherent characteristics result in a low power factor, leading to ineffectiveness and enlarged energy consumption [3, 4]. The low power factor in IMs is primarily caused by the reactive power component, which leads to an imbalance between real and apparent power. This imbalance increases current flow and losses in the electrical system, reducing overall Efficiency [5, 6]. PFC techniques aim to minimalize the reactive power and transport the power factor closer to unity, thus improving the Efficiency and performance of IM systems [7-9]. The conventional power factor correction techniques, which typically employ isolated converters, have limitations such as high voltage stress on the bridge rectifier and increased conduction losses [10]. Table 1 represents the literature summary of conventional converters as described as follows. To address these challenges, the non-isolated bridgeless high-gain SEPIC converter for PFC is introduced in this proposed work. This converter topology offers advantages such as galvanic isolation between the input and output, allowing for flexible voltage conversion. Also, the bridgeless configuration eliminates the need for a bridge rectifier, reducing voltage

stress and improving overall converter efficiency. On the other hand, the control approach is required to regulate the converter's performance [16]. Thus, the PI controller [17] is used generally for controlling the converter and for fine-tuning these control parameters, the optimization algorithm is crucial [18].

Hence, the existing topologies like GA [19], PSO [20] are utilized for tuning the parameters of the PI controller efficiently by providing better settling time and robustness [21]. However, it has drawbacks like low convergence rate in iterative process, high complexity and high computational cost [22, 23].

Table 1. Summary of existing converters for PFC

Reference	Methodology	Advantages	Limitations
Ortiz-Castrillón et al (2021) [11]	Semi-Bridgeless Boost Converter	The conduction losses are reduced by this technique, thereby increasing the overall Efficiency.	It is preferable to utilize non-linear controllers with a high operating range and quick response time to enhance the response of power systems.
Majida Kazmie et al (2021) [12]	AC-DC PFC Cuk converter	It guarantees a power factor that is almost equal to unity and a low overall harmonic distortion in the current.	The overall higher component count and cost lead to power consumption.
Tanmay et al (2023) [13]	bridgeless buck boost-Cuk	It is more efficient, has fewer components, and improves power quality.	The disadvantage of this method is the greater current stress imposed by a lower amount of inductance.
Sivamani et al (2021) [14]	SEPIC converter for PFC	The overall THD is reduced with unity PF.	It has high complexity and voltage stress.
Benisha et al (2022) [15]	Interleaved Boost Integrated Flyback Converter for PFC	Voltage ripples and harmonics are mitigated by using this converter to decrease the THD level	They require additional current control loops for active current balancing, which can increase complexity.

In order to overcome the above-stated problems, the developed approach incorporates the CPSO-PI controller to regulate and control the power factor correction process.

It combines the benefits of constricted particle swarm optimization, a metaheuristic optimization algorithm, with a proportional-integral control strategy. The contributions of the developed work are demonstrated below.

- A non-isolated PFC technique has been developed to improve the power quality of IM applications.
- The bridgeless SEPIC converter is used to reduce conduction losses, increase the overall Efficiency of the PFC system, and make it suitable for IM applications.
- A CPSO algorithm is proposed to optimize the PI controller parameters to achieve enhanced dynamic response and to ensure better convergence and stability, with reduced computational cost.

The overall proposed work is executed in MATLAB/Simulink to validate the efficacy of the developed work.

2. Proposed Methodology

Power factor correction is crucial in electrical systems to ensure efficient utilization of power and minimize energy losses. Conventional PFC techniques often rely on isolated converters, which introduce additional components like transformers, resulting in increased size, weight, and cost. The proposed technique utilizes a novel bridgeless high-gain SEPIC converter with CPSO-PI controller for IM applications to overcome these limitations. The block diagram of the developed work is represented in Figure 1, and the detailed explanation is given under the figure as follows.

The AC supply is provided as the input to the system, which is connected to the bridgeless SEPIC converter, a non-isolated power converter. The converter performs PFC and boosts the voltage to a higher level. The CPSO-PI controller is developed to regulate the operation of a bridgeless SEPIC converter with stable voltage. The CPSO algorithm optimizes the control parameters of the PI controller, ensuring accurate and efficient power factor correction.

The PWM generator generates the PWM signals based on the control signals from the CPSO-PI controller, which control the switching operation of the bridgeless SEPIC converter, enabling precise control of the output voltage. The output of the bridgeless SEPIC converter, which is a DC, is fed into a phase VSI that converts the DC into AC to supply power to the IM.

The PI controller controls the operation of the IM, regulating the output voltage and maintaining stable and efficient performance of the IM. Finally, the IM receives the controlled and uninterruptible AC power through the inverter, allowing its operation to have an improved power factor and Efficiency.

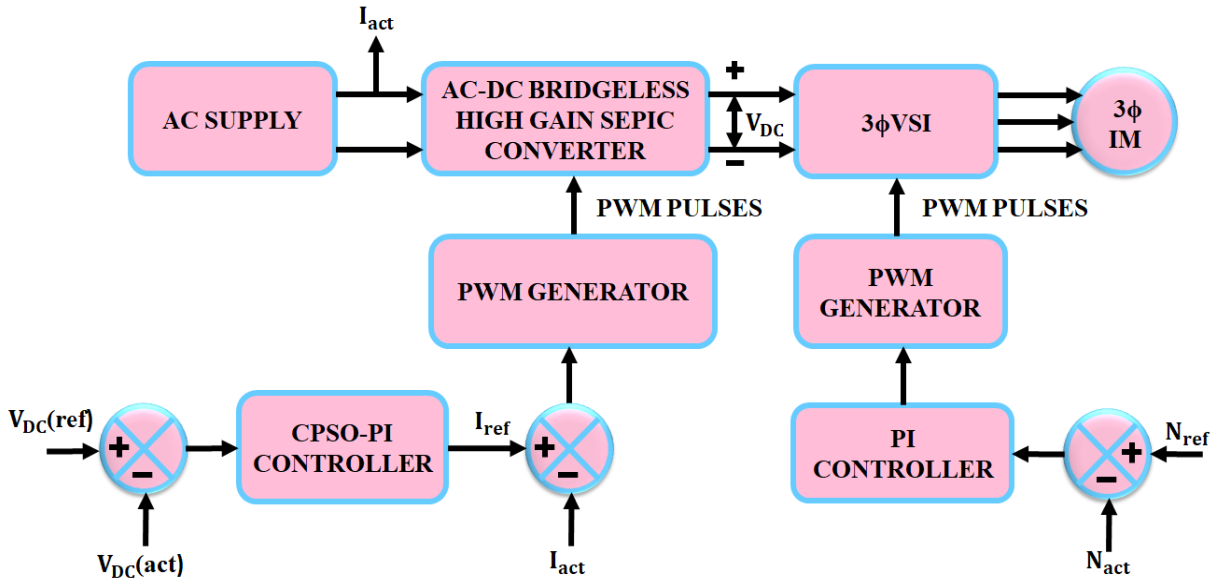

Fig. 1 Proposed block diagram

2.1. Modelling of High-Gain Bridgeless SEPIC Converter

This research proposes a novel bridgeless PFC circuit based on a SEPIC converter, as displayed in Figure 2, which operates in Discontinuous Conduction Mode (DCM) since this mode type has many benefits, including decreased component stress, inherent PFC operation, and suitability for low power applications. The developed converter's circuit operation is separated into three subinterval modes, Mode 1, Mode 2 and Mode 3 as represented in Figure 3.

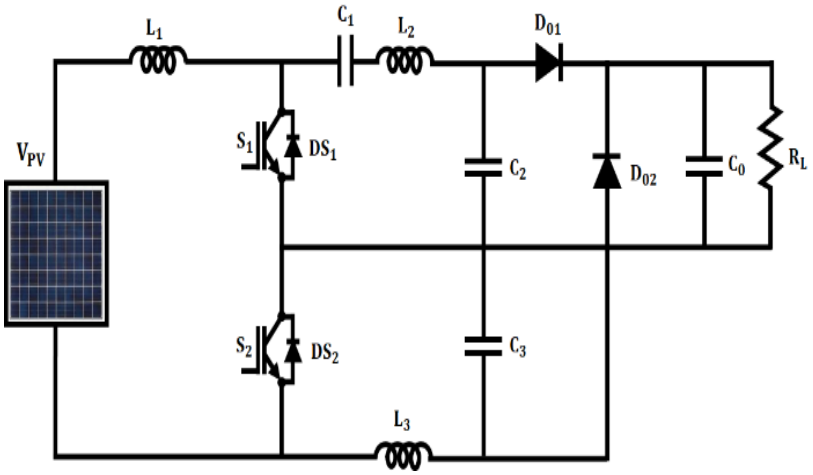

Fig. 2 Circuit diagram of high-gain Bridgeless SEPIC converter

Mode 1: In this state, the switch S_1 In the ON condition and S_1 It is in the OFF state, and the current is flowing from the source. V_{PV} , which passes via the input inducer. Concurrently, as Figure 3(a) illustrates, the current over L_1 enlarged linearly to its maximum. The second inducer L_2 discharged its energy linearly to C_{b1} and made a current path to s_1 before flowing back to L_2. The output diode, D_{O1} is reverse-bias at this moment, at the output voltage equals the capacitor voltage V_O. The duty cycle is represented by the letter. d_1,

$$i_{L1-peak} = \frac{v_g}{L_1}(d_1 T_s) \quad (1)$$

Mode 2: The circuit in Mode 2 is seen in Figure 3(b). In this condition, S_1 It is obviously shut off, preventing any current from passing through it and S_2 is turned ON also, D_{O1} It is now forward-bias. At this point, the process of releasing its current to the load over iC_{b1} as well as iD_{O1} making the return channel through D_{S2} causes the current through L_1 to fall linearly along with V_{PV}. L_2 Simultaneously discharge its current linearly to the load via iD_{O1}. Now, the sum of iL_1 and iL_2 passing the current through D_{O1}. Consequently, D_{O1} The peak current is given as,

$$i_{Do1-pk} + i_{L2-pk} = d_1 T_s \left[\frac{v_g}{L_1} + \frac{v_{cb1}}{L_2}\right] \quad (2)$$

$v_{cb1} \approx v_g$ is simplified by the following Equation (3),

$$i_{Do1-pk} = d_1 T_s \left[\frac{v_g}{L_a}\right] \quad (3)$$

Here $L_a = L_1/L_2$. By analyzing the ripple current atL_1, the d_2 *The* width is ascertained in this way:

$$d_2 = \frac{v_g}{(v_{cb1}+v_o-v_g)} d_1 \quad (4)$$

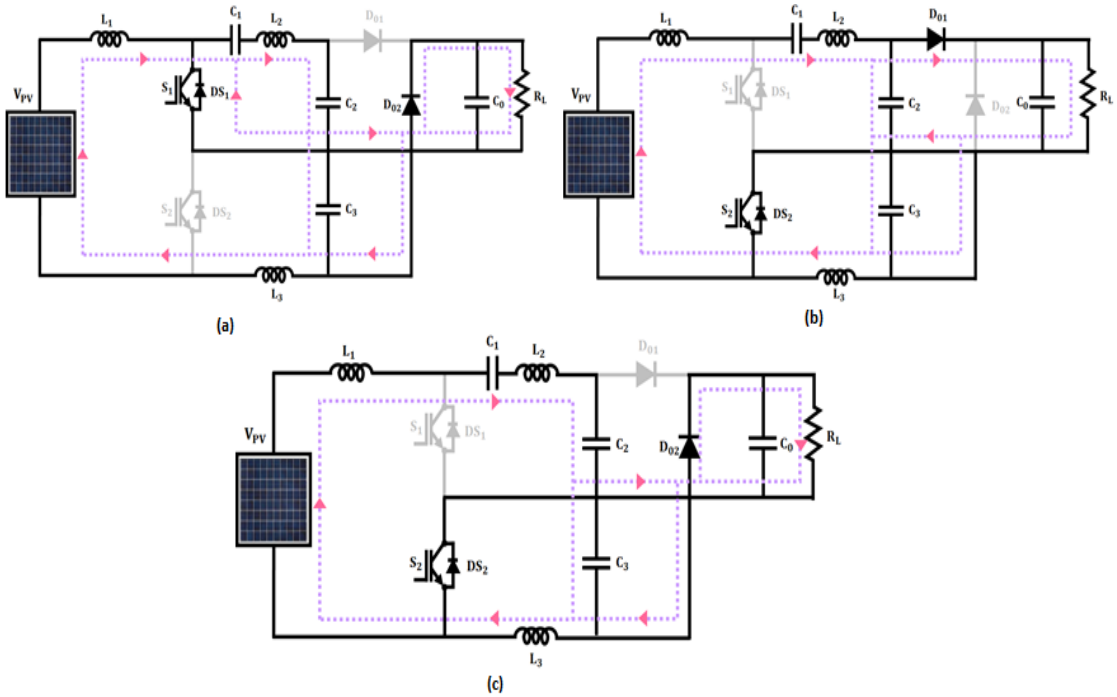

Fig. 3 Modes of operation, (a) Mode 1, (b) Mode 2, and (c) Mode 3.

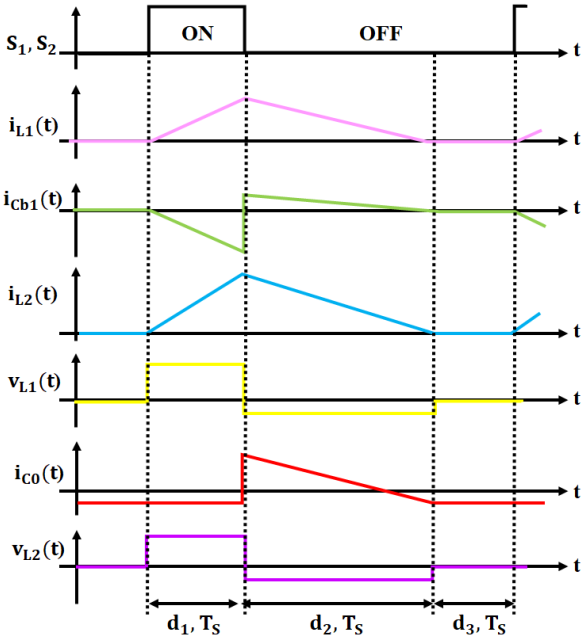

Fig. 4 Switching operation of the proposed converter

Mode 3: Ultimately, S_1 and D_{01} They are both disabled in this mode, leaving just two closed current paths at the input and output sides. At this moment, V_{PV} equals VC_{b1}, and it is assumed that the energy at L_1 and L_2 is equal. Consequently, the input current is almost equivalent to zero. Nevertheless, there is a virtual DC current present in this mode, and the current flows in the opposite direction, but at equal amounts through L_1 andL_2.

The relationship between input and output voltage, or more often termed as the voltage conversion ratio, is found by equating the average current of D_{01} With the output current, $i_O = \frac{V_O}{R}$

$$M = \frac{v_o}{v_g} = d_1 \sqrt{\frac{RT_s}{2L_a}} \quad (5)$$

Where R represents the resistive load. Conversely, in order to guarantee DCM functioning during every switching interval, the component choice needs to adhere to this formula:

$$1 - d_1 > \sqrt{\frac{2L_a}{RT_s}} \quad (6)$$

A dotted line depicted in Figure 5 can be used to represent the boundary between CCM and DCM functions by utilizing Equation (6). Operation in the CCM region occurs when the converter operates above the dotted line; operation in the

DCM region occurs when it operates below the dotted line. Therefore, it is clear from the figure that the converter will either function in CCM or DCM under any load state when it operates at a specific duty cycle and input voltage value. To ensure DCM operation in this work, an appropriate duty cycle and load condition are established initially.

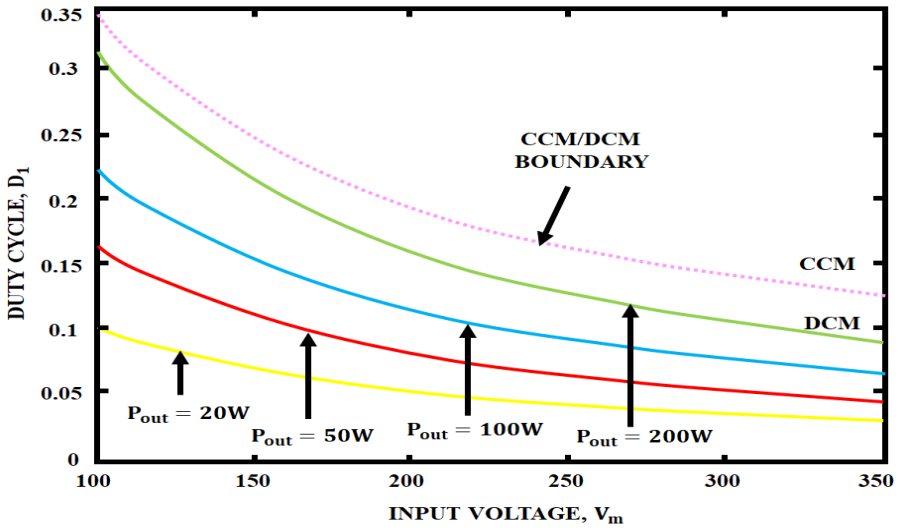

Fig. 5 Boundary condition of CCM and DCM

The enhanced and high-voltage gain with unity PF is achieved by the developed high-gain bridgeless SEPIC converter. Moreover, the control approach is crucial for stabilizing the voltage; thus, the CPSO-PI controller is employed, as explained below.

2.2. Modelling of Chaotic PSO-Based PI Controller

The simplicity and Efficiency of the PI controller in managing steady-state errors make it a popular choice for control systems. While the integral control constantly modifies the control signal to eliminate any residual steady-state error, the proportional control delivers a quick initial reaction to minimize error. Optimization techniques are employed to determine the optimal or near-optimal ideals for the PI controller's gain parameters. The main goal is to achieve the best control performance and meet specific system requirements. A Chaotic PSO-PI controller refers to a control algorithm combining PSO, PI control, and chaos theory. It is used to optimize the performance of control systems. The basic idea behind a Chaotic PSO-PI controller is to introduce chaotic behavior into the PSO algorithm to enhance its exploration and exploitation capabilities, leading to improved control performance. Chaos theory emphasizes the inherent randomness and sensitivity to initial conditions in dynamic systems. By incorporating chaotic elements into the PSO algorithm, the controller can better explore the solution space and find optimal or near-optimal control parameters. Every time the algorithm iterates, better results are produced and new solutions are suggested. Basic demographic data is generated at random. Subsequently, each iteration's information is generated by utilizing the data from its predecessor. A particle's velocity is another essential characteristic, in addition to its position. The direction and range of a particle's move in each iteration are determined by its velocity, which is represented by a vector. Each particle's position in the j+1th iteration is determined by

$$x_i^{j+1} = x_i^{j} + v_i^{j+1} \tag{7}$$

For each particle in the $j+1$ iteration, denoted by V^{j+1}. Every particle is moved in each iteration by the same amount as its velocity vector from the previous iteration. Each particle's choice for its subsequent iterations affects how fast that particle moves. Therefore, in $j+1$ iteration, the velocity of each particle can be computed as

$$v_i^{j+1} = w.v_i^{j} + r_1.C_1.(x_i^{pbest} - x_i^{j}) + r_2.C_2.(x_i^{gbest} - x_i^{j}) \tag{8}$$

PSO commonly makes use of the logistic map, a component of population dynamics. The following defines the logistic equation.

$$x_{n+1} = \mu x_n(1 - x_n), 0 \le x_n \le 1 \tag{9}$$

When n = 0, 1, 2, and x is a variable, and μ is the control parameter. The chaotic local search procedure could be described by the following formula:

$$cx_i^{(k+1)} = 4cx_i^{(k)}\left(1 - cx_i^{(k)}\right), i = 1,1, \ldots n \tag{10}$$

Where k signifies a number of iterations and cx_i is the i^{th} The chaotic variable and the flowchart of the proposed CPSO are represented in Figure 6.

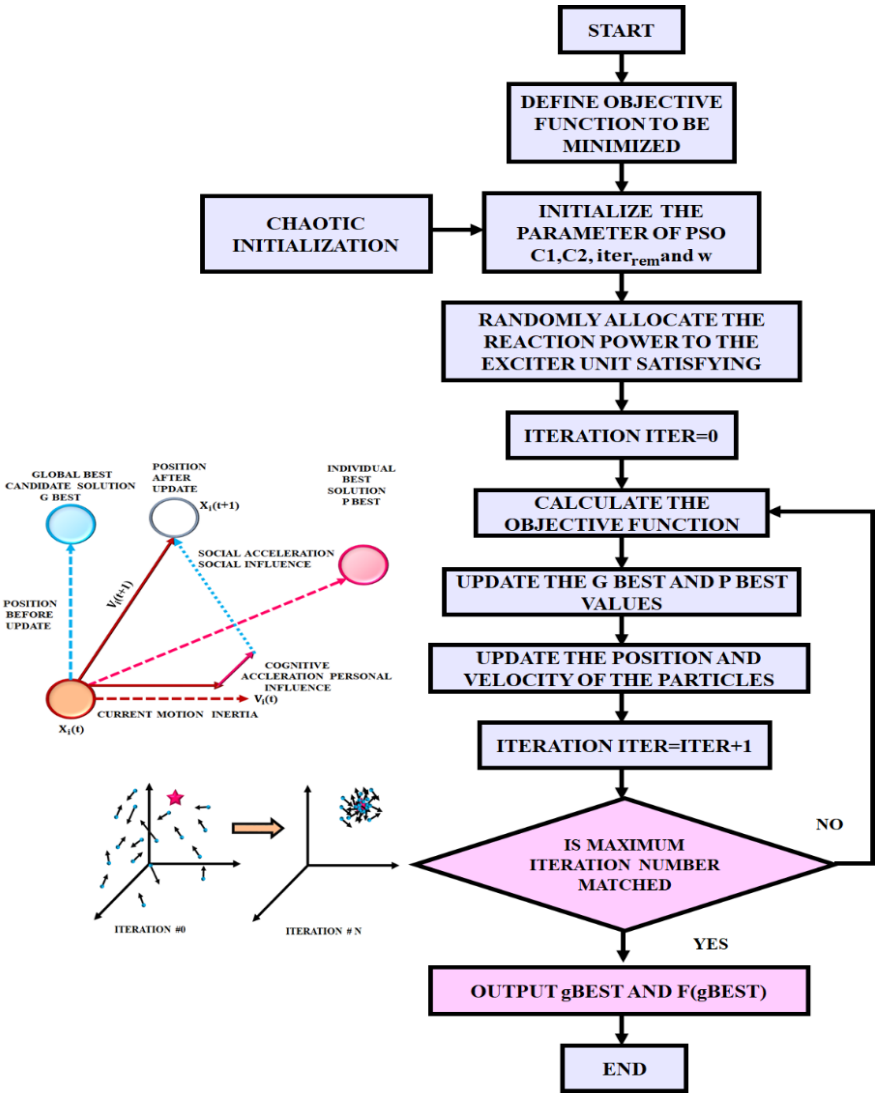

Fig. 6 Flowchart of proposed CPSO-PI controller

The following serves as an illustration of how chaotic local search works:

Step 1 : Assuming $k = 0$, apply the following equation to transfer the decision variables $cx_i^{(k)} = 1, 2\ldots n$ among the intervals $(x_{min,i}, x_{max,i})$ to chaotic variables $cx_i^{(k)}$ At interval (0, 1).

$$cx_i^{(k)} = \frac{x_i^{(k)} - x_{min,i}}{x_{max,i} - x_{min,i}}, \quad i = 1,2,\ldots n \tag{11}$$

Step 2 : Using the logistic equation in accordance with $cx_i^{(k)}$ to determine the chaotic variables $cx_i^{(k+1)}$ for the following iteration.

Step 3 : Applying the following formula to change the chaotic variables $cx_i^{(k+1)}$ to decision variables $x_i^{(k+1)}$

$$x_i^{(k+1)} = x_{min,i} + cx_i^{(k+1)}\left(x_{max,i} - x_{min,i}\right), \quad i = 1,2,..,n \tag{12}$$

Step 4 : Assessing the novel resolution utilizing decision variables $x_i^{(k+1)}$.

Step 5 : As a result of the chaos search, output the new solution if it outperforms the non-chaos search solution or if the predetermined maximum iteration is reached; if not, let $k = k + 1$ and return to Step 2.

The optimal area cannot be searched in a short amount of time if the search space is too large.

Therefore, the chaotic search is conducted in a narrow range to achieve high performance. The following formulae are used to modify this search area.

$$x_{min,i} = max(x_{min,i}, x_g - r(x_{max,i} - x_{min,i})) \quad (13)$$

$$x_{max,i} = min(x_{max,i}, x_g - r(x_{max,i} - x_{min,i})) \quad (14)$$

Where r is a variable with a value between 0 and 1, and x_g It is the current global best position. The Efficiency of the search will rise if the chaotic search's range is reduced. By utilizing the proposed CPSO algorithm, the PI parameters get optimally tuned with better convergence rate, settling time, computational cost and system stability.

2.3. Modelling of Induction Motor

Asynchronous motors, also referred to as three-phase IMs, are a common class of electric motor applied in a wide range of profitable and industrialized situations. It uses a revolving magnetic field and electromagnetic induction to transform electrical energy into mechanical energy. The synchronous rotating speed reference frame is used in the motor model equations to ensure that all input voltages are constants in the dq domain. The following shows the electrical balancing formula for an IM's stator phase, displayed in the ABC reference frame:

$$u_A = r_A i_A + \frac{d\psi_A}{dt} \quad (15)$$

Elements from the coupling, as well as leakage magnetic flux, make up the A-phase. L_{AA} Self-inductance of a stator. Examining the primary magnetic flux inductance for a stator phase (L_m) and the single-phase inductance L_{ms}.

$$L_m = \frac{3}{2} L_{ms} \quad (16)$$

A similar ratio for $L_{\sigma s}$ The leaking inductance is expressed as,

$$L_{AA} = \frac{2}{3}(L_m + L_{\sigma s}) \quad (17)$$

The parameters of a similar circuit can be usefully employed for simulating an IM, and there is a simple way to do it. In order to calculate the mutual inductance between the stator windings, the following formula is applied, assuming that they are symmetric:

$$L_{AB} = L_{AC} = L_{AA} \cos\frac{2\pi}{3} = -\frac{1}{3}(L_m + L_{\sigma s}) \quad (18)$$

A stator winding, also referred to as a rotor phase, can be expressed as (11):

$$u_a = r_a i_a + \frac{d\psi_a}{dt} \quad (19)$$

Considering the self-inductance L_{aa} of a rotor phase, mutual inductances L_{ab}, L_{ac} across rotor windings, mutual inductances L_{Aa},L_{Ab} and L_{Ac} Between the rotor and stator, the flux linkage is derived. $\frac{d\psi_a}{dt}$ It is comparable to (15).

Much like in Equation (17), the turn ratio k is used to determine the self-inductance of a rotor phase.

$$L_{aa} = \frac{2}{3k^2}(L_m + L_{\sigma r}) \quad (20)$$

When rotor windings are symmetric, the mutual inductance shows,

$$L_{ab} = L_{ac} = L_{aa} \cos\frac{2\pi}{3} = -\frac{1}{3k^2}(L_m + L_{\sigma r}) \quad (21)$$

Finally, by employing the proposed converter and control approach, the IM motor can be run without any distortions and interruptions.

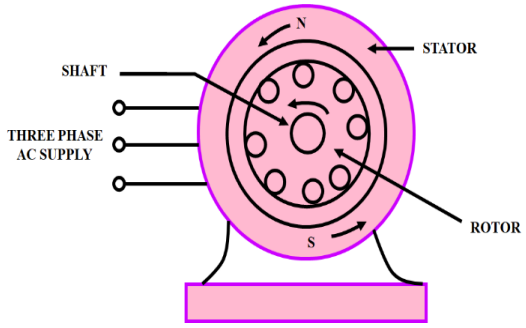

Fig. 7 Three-phase IM

3. Results and Discussion

This section discusses the results obtained from MATLAB/Simulink for the proposed technique. The performance of the developed PFC bridgeless high-gain SEPIC converter is evaluated in terms of power factor correction, input current harmonics, output voltage regulation, and Efficiency. Also, the CPSO-PI controller employed in the proposed method is evaluated in terms of settling time, convergence speed, and robustness. Additionally, a comparative study is conducted with existing approaches to assess the performance of the developed work and the parameter specification for the developed work is represented in Table 2.

Table 2. Parameter specifications for the proposed work

Bridgeless SEPIC-Cuk converter	
Parameter	Values
Input AC supply range (V_{AC})	$180 - 270V$
Input power rating	1kW

Output DC voltage range (V_{DC})	270 – 330V
L_1, L_2, L_3	1mH
C_1, C_2	2.36µF
C_O	2200µF
Diode	IN4148
Controller	FPGA Spartan 6E
Driver Circuit	TLP250
3ϕ Induction Motor	
Parameters	Values
Power	1Hp
Speed	1390 rpm
Voltage	415V (AC)
No. of poles	4
Frequency	50 Hz

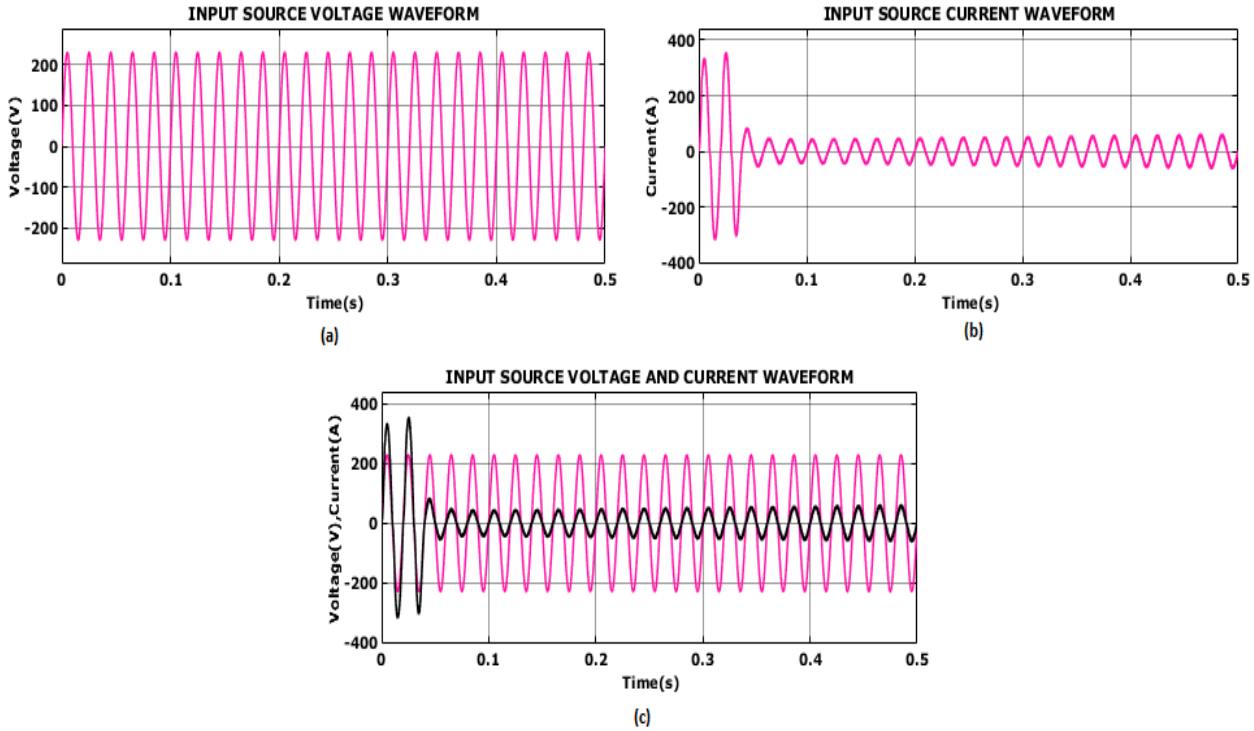

Fig. 8 Input source waveform for (a) Voltage, (b) Current, and (c) Voltage and current.

The input voltage source waveform maintains a constant voltage level of 210V throughout its entire duration, which contributes to the constancy and dependability of the overall system as represented in Figure 8(a).

Similarly, the current waveform as indicated in Figure 8(b) specifies that it fluctuates during the initial period and after 0.3s, the constant current is stabled at 20A.

Furthermore, the in-phase of voltage and current is illustrated in Figure 8(c), which maintains a constant voltage and current at 210V and 20A, respectively. Figure 9 represents the power factor waveform, which illustrates that the PFC maintains its unity.

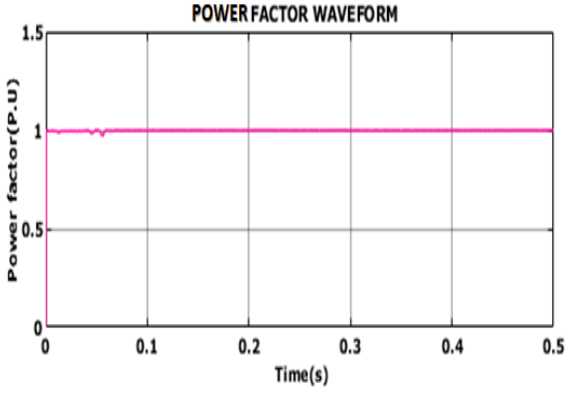

Fig. 9 Power factor waveform

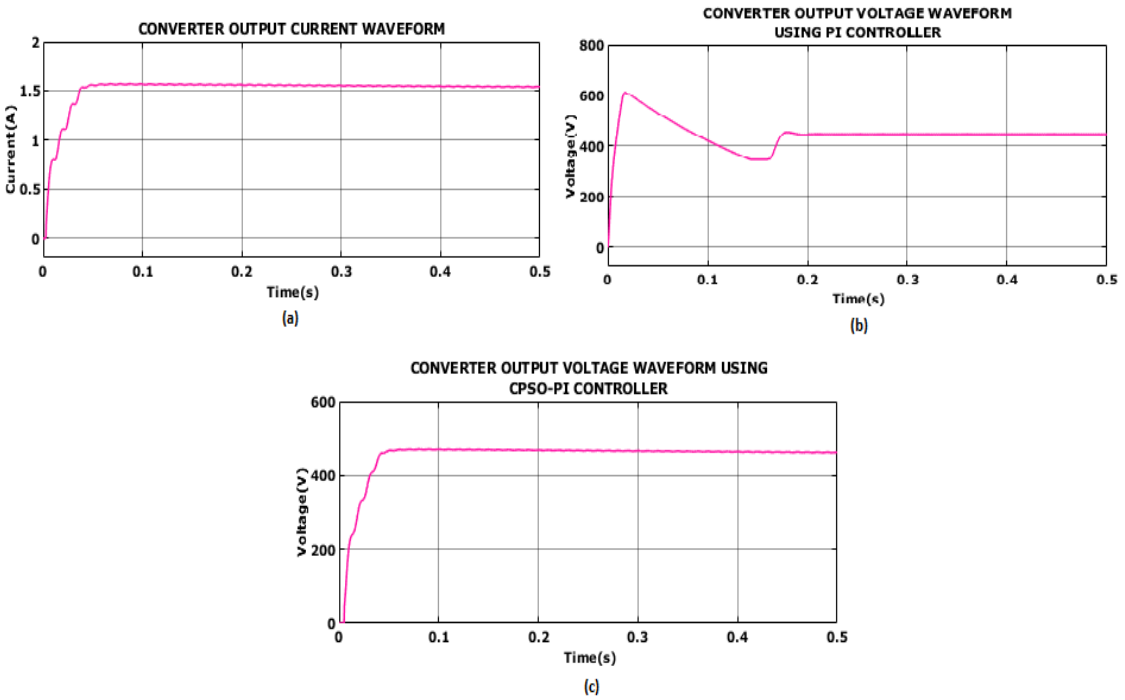

Fig. 10 Converter output waveform, (a) Current, (b) Voltage using PI controller, and (c) Voltage using CPSO-PI controller.

The converter output current waveform is shown in Figure 10, which identifies that the proposed converter current oscillated initially. After that,onstis was antly stable at 1.6A. Byzantizing the PI controller, similarly, adopting the proposed CPSO-PI controller fluctuated during the initial period up to 0.1s, and it is constantly stabilized at 540V, respectively.

3.1. Case 1 at Load 1.5 N-M

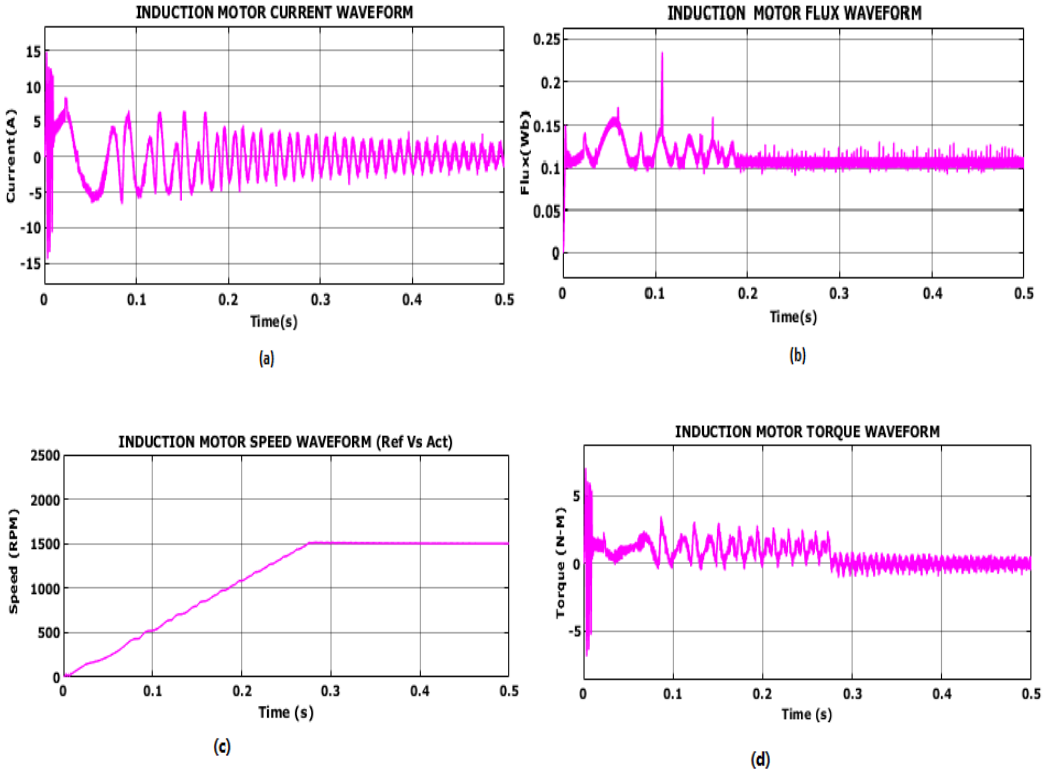

Fig. 11 Induction motor waveform, (a) Current, (b) Flux, (c) Speed, and (d) Torque for case 1.

The IM current for case 1 is specified in Figure 11, which analyze that the current varies up to 0.4s after that it is continually sustained at 3 to -3A as specified in Figure 11(a). Similarly, the flux waveform illustrated in Figure 11(b) is constantly stabilized at 0.1Wb after varying up to 0.3s. The IM speed waveform is represented in Figure 11(c), where it is observed that the speed of IM is constantly stable at 1500RPM after oscillating for some time. Furthermore, the IM torque waveform is indicated in Figure 11(d). From the result, it is obvious that the torque in IM has remained constant at 2 (N-M) after fluctuating for some duration in the initial period.

3.2. Case 2 at Load 2N-M

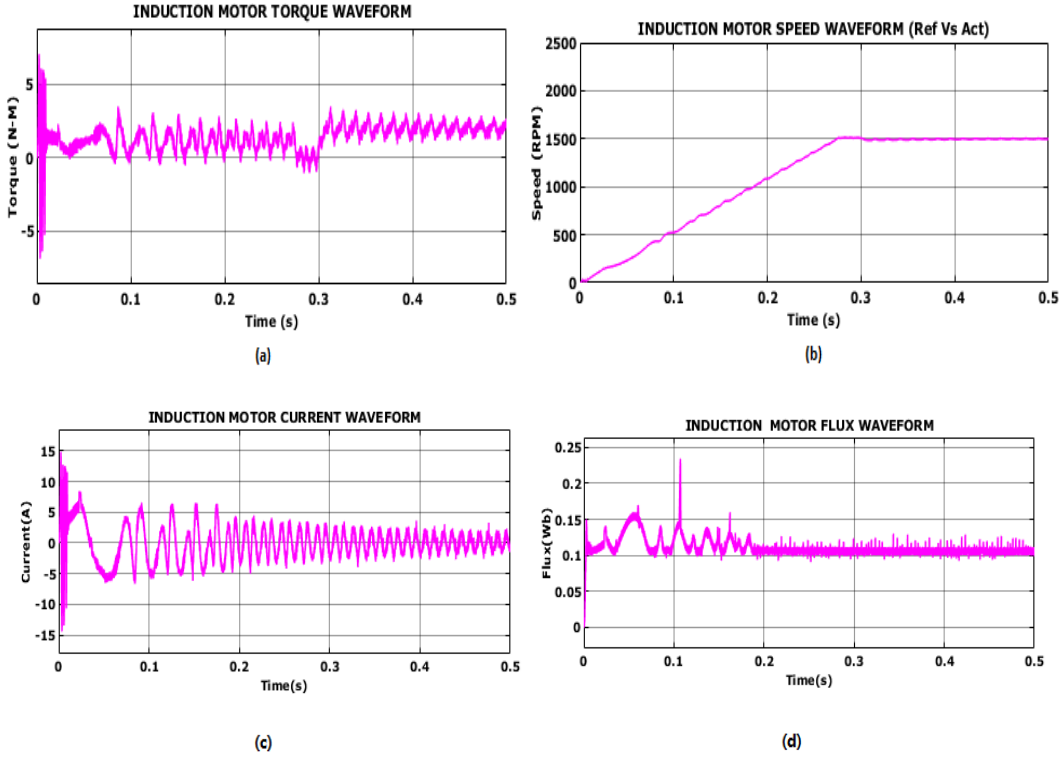

Fig. 12 Induction motor waveform, (a) Current, (b) Flux, (c) Speed, and (d) Torque for case 2.

The torque waveform of the IM, indicated in Figure 12(a), clearly shows that the torque maintains a constant value at 2.1(N · m) after experiencing fluctuations during the initial period. The speed waveform of the IM, as indicated in Figure 12(b), demonstrates that the motor's speed stabilizes at 1500 RPM after undergoing oscillations for a considerable period of time.

The current waveform of IM in case 2 exhibits initial fluctuations for a duration of up to 0.4 seconds. However, the current stabilizes beyond this period and remains constant at 3 to -3A. Similarly, the flux waveform, as depicted in the corresponding Figure 12(d), initially experiences variations until approximately 0.3 seconds, reaching a stable state of 0.1Wb.

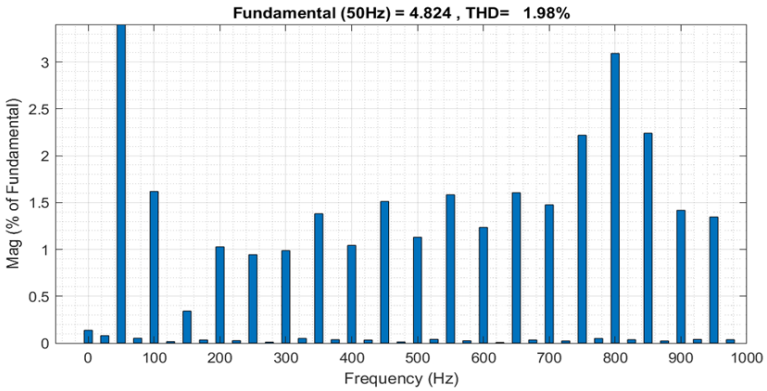

Fig. 13 THD waveform for the proposed high-gain converter

The THD waveform for the proposed work is shown in Figure 13, which represents the High Gain Bridgeless SEPIC converter, with a THD value of 1.98%, which is satisfied by the IEEE standards. The comparison of THD is represented in Figure 14, which analyze that the proposed bridgeless high-gain SEPIC converter attains low THD compared to other listed approaches, as indicated in the above graph. Similarly, the developed converter is compared with the conventional converters to determine better Efficiency. As signified in Table 3, it is clear that the developed converter has a better Efficiency of 96.57% compared to others.

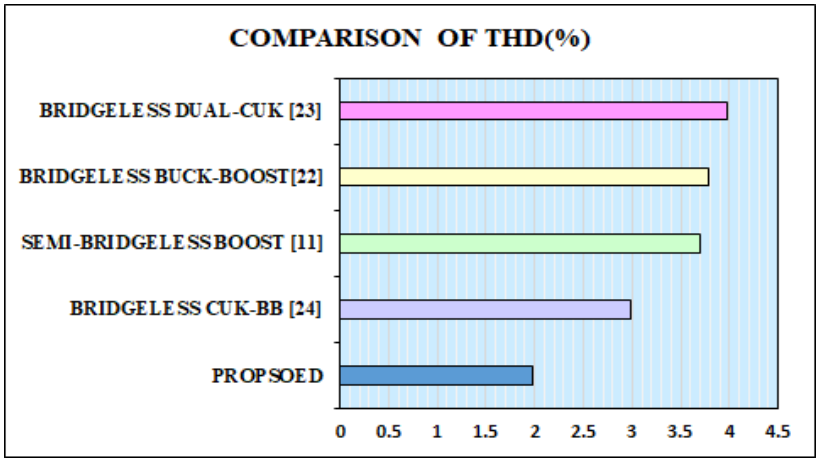

Fig. 14 Comparison of THD

Table 3. Comparison of efficiency

Converters	Efficiency (%)
[13]	92%
[23]	96.1
[24]	95%
Proposed high-gain converter	96.57%

The proposed CPSO-PI controller is compared with the normal PI controller as represented in Table 4, which shows that the developed control topology attains better settling time, rise time and peak overshoot.

Table 4. Evaluation of the controller

Controllers	Settling Time(s)	Rise Time (s)	Peak overshoot (%)
PI	0.2s	0.02s	0.03
CPSO-based PI	0.1s	0.01s	0.01

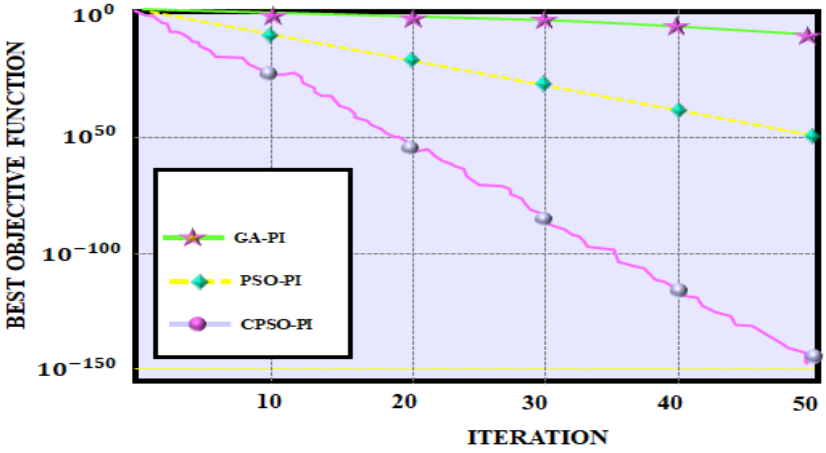

Fig. 15 Comparison of convergence speed

The conventional GA-PI and PSO-PI are compared with the proposed CPSO-PI to prove the prominence of the developed optimized control strategy. The graph shows that the developed topology attains a better convergence rate than the others, as illustrated in Figure 15.

4. Conclusion

A novel high-gain bridgeless SEPIC converter with CPSO-PI controller is proposed in this paper for IM Applications. The utilization of a bridgeless high-gain SEPIC converter, along with the CPSO-PI controller, ensures

enhanced PFC. Moreover, the improved power factor and Efficiency lead to increased power quality, reducing harmonic distortion and enhancing the electrical grid's stability. Overall, this approach is applied in MATLAB/Simulink to show the prominence of the developed work. As a result, it is observed that the proposed converter and control approach achieves a better THD of 1.98%, Efficiency of 96.57% with unity PF and a settling time of 0.1s with a rapid convergence rate compared to the other techniques. Thereby, this solution enhances the Efficiency and performance of induction motors, leading to reduced power losses and increased power quality. Therefore, it is considered a viable and advantageous option for power factor correction in induction motor applications.

References

[1] Zeineb Ben Safia et al., "TS Fuzzy Fault-Tolerant Tracking Control of a PV Pumping System Based on an Induction Motor," *IETE Journal of Research*, vol. 69, no. 7, pp. 4826-4835, 2023. [CrossRef] [Google Scholar] [Publisher Link]

[2] Rashmi Rai, Saurabh Shukla, and Bhim Singh, "Sensorless Field Oriented SMCC Based Integral Sliding Mode for Solar PV Based Induction Motor Drive for Water Pumping," *IEEE Transactions on Industry Applications*, vol. 56, no. 5, pp. 5056-5064, 2020. [CrossRef] [Google Scholar] [Publisher Link]

[3] Shaikh Mohammed Suhel, and Rakesh Maurya, "A New Switching Sequences of SVPWM For Six-Phase Induction Motor with Features of Reduced Switching Losses," *CES Transactions on Electrical Machines and Systems*, vol. 5, no. 2, pp. 100-107, 2021. [CrossRef] [Google Scholar] [Publisher Link]

[4] Utkal Ranjan Muduli et al., "Direct Torque Control with Constant Switching Frequency for Three-to-Five Phase Direct Matrix Converter Fed Five-Phase Induction Motor Drive," *IEEE Transactions on Power Electronics*, vol. 37, no. 9, pp. 11019-11033, 2022. [CrossRef] [Google Scholar] [Publisher Link]

[5] Jamal Abdul-Kareem Mohammed, Sahar R. Al-Sakini, and Arkan Ahmed Hussein, "Assessment of Disturbed Voltage Supply Effects on Steady-State Performance of an Induction Motor," *International Journal of Electrical and Computer Engineering*, vol. 10, no. 3, pp. 2259-2270, 2020. [CrossRef] [Google Scholar] [Publisher Link]

[6] Horia Gheorghe Beleiu et al., "Harmonics Consequences on Drive Systems with Induction Motor," *Applied Sciences*, vol. 10, no. 4, pp. 1-15, 2020. [CrossRef] [Google Scholar] [Publisher Link]

[7] Shoaib Shaikh et al., "Protection System Design of Induction Motor for Industries," *Modelling and Simulation in Engineering*, vol. 2022, pp. 1-13, 2022. [CrossRef] [Google Scholar] [Publisher Link]

[8] Gowthamraj Rajendran et al., "Voltage Oriented Controller Based Vienna Rectifier for Electric Vehicle Charging Stations," *IEEE Access*, vol. 9, pp. 50798-50809, 2021. [CrossRef] [Google Scholar] [Publisher Link]

[9] Hichem Hamdi, Chiheb Ben Regaya, and Abderrahmen Zaafouri, "A Sliding-Neural Network Control of Induction-Motor-Pump Supplied by Photovoltaic Generator," *Protection and Control of Modern Power Systems*, vol. 5, no. 1, pp. 1-17, 2020. [CrossRef] [Google Scholar] [Publisher Link]

[10] R. Suguna et al., "A Non-Isolated PFC Bridgeless SEPIC-Cuk Converter with Adaptive PI Controller for Induction Motor," *International Journal of Applied Power Engineering (IJAPE)*, vol. 13, no. 2, pp. 282-293, 2023. [CrossRef] [Google Scholar] [Publisher Link]

[11] José Robinson Ortiz-Castrillón et al., "A Sliding Surface for Controlling a Semi-Bridgeless Boost Converter with Power Factor Correction and Adaptive Hysteresis Band," *Applied Sciences*, vol. 11, no. 4, pp. 1-21, 2021. [CrossRef] [Google Scholar] [Publisher Link]

[12] Hashim Raza Khan et al., "An Isolated Power Factor Corrected Cuk Converter with Integrated Magnetics for Brushless DC Ceiling Fan Applications," *Electronics*, vol. 10, no. 14 pp. 1-24, 2021. [CrossRef] [Google Scholar] [Publisher Link]

[13] Tanmay Shukla, Narayan Prasad Patidar, and Apsara Adhikari, "A Power Factor Profile-Improved EV Charging System Using Bridgeless Buckboost-Cuk Converter," *International Transactions on Electrical Energy Systems*, vol. 2023, pp. 1-15, 2023. [CrossRef] [Google Scholar] [Publisher Link]

[14] D. Sivamani et al., "Design and Implementation of Highly Efficient UPS Charging System with Single Stage Power Factor Correction Using SEPIC Converter," *Materials Today: Proceedings*, vol. 45 pp. 1809-1819, 2021. [CrossRef] [Google Scholar] [Publisher Link]

[15] S. Benisha, and J. Anitha Roseline, "Interleaved Boost Integrated Flyback Converter for Power Factor Correction in Brushless DC Motor Drive," *Intelligent Automation & Soft Computing*, vol. 33, no. 3, pp. 1363-1378, 2022. [CrossRef] [Google Scholar] [Publisher Link]

[16] Eduardo Quintero-Manríquez et al., "Neural Control of an Induction Motor with Regenerative Braking as Electric Vehicle Architecture," *Engineering Applications of Artificial Intelligence*, vol. 104, 2021. [CrossRef] [Google Scholar] [Publisher Link]

[17] Antony K. Peter, Jaison Mathew, and K. Gopakumar, "A Simplified DTC-SVPWM Scheme for Induction Motor Drives Using a Single PI Controller," *IEEE Transactions on Power Electronics*, vol. 38, no. 1, pp. 750-761, 2023. [CrossRef] [Google Scholar] [Publisher Link]

[18] Abha Pragati, Bibhu Prasad Ganthia, and Bibhu Prasad Panigrahi, "Genetic Algorithm Optimized Direct Torque Control of Mathematically Modeled Induction Motor Drive Using PI and Sliding Mode Controller," *Recent Advances in Power Electronics and Drives: Select Proceedings of EPREC 2020*, pp. 351-366, 2021. [CrossRef] [Google Scholar] [Publisher Link]

[19] Hector Fretes et al., "Pareto Optimal Weighting Factor Design of Predictive Current Controller of a Six-Phase Induction Machine Based on Particle Swarm Optimization Algorithm," *IEEE Journal of Emerging and Selected Topics in Power Electronics*, vol. 10, no. 1, pp. 207-219, 2022. [CrossRef] [Google Scholar] [Publisher Link]

[20] Mohamed Elgbaily, Fatih Anayi, and Michael Packianather, "Genetic and Particle Swarm Optimization Algorithms Based Direct Torque Control for Torque Ripple Attenuation of Induction Motor," *Materials Today: Proceedings,* vol. 67, pp. 577-590, 2022. [CrossRef] [Google Scholar] [Publisher Link]

[21] M.A. Hannan et al., "Role of Optimization Algorithms Based Fuzzy Controller in Achieving Induction Motor Performance Enhancement," *Nature communications*, vol. 11, no. 1, pp. 1-11, 2020. [CrossRef] [Google Scholar] [Publisher Link]

[22] T. Vijayalakshmi et al., "A Power Factor Corrected Bridgeless Buck-Boost Converter-Fed Brushless Direct Current Motor Drive with Fuzzy Controller," *Turkish Journal of Computer and Mathematics Education (TURCOMAT)*, vol. 12, no. 13, pp. 228-236, 2021. [Google Scholar] [Publisher Link]

[23] K.V. Gopan, and J.D. Shree, "Implementation of a High Power Quality BLDC Motor Drive Using Bridgeless DC to DC Converter with Fuzzy Logic Controller," *Engineering, Technology & Applied Science Research*, vol. 12, no. 5, pp. 9178-9185, 2022. [CrossRef] [Google Scholar] [Publisher Link]

[24] Tanmay Shukla, and Srete Nikolovski, "A Bridgeless Cuk-BB-Converter-Based BLDCM Drive for MEV Applications," *Energies*, vol. 16, no. 9, pp. 1-20, 2023. [CrossRef] [Google Scholar] [Publisher Link]